Nathanael Zhixin Wong
nathanaelwong@fas.harvard.edu



# The Dynamics of Aquaplanet Monsoons and their dependence on Axial Tilt and Slab Depth

**Last Modified:** 18th May, 2020

**Abstract**

In this project, I run Aquaplanet GCM simulations with varying axial tilt and ocean slab depth to investigate the dependence of monsoon dynamics and the transition of the Hadley Cell between the **equinoctal** (eddy-momentum dependent) and **soltitial** (angular-momentum-conserving) regimes states, and replicate some of the work that was done by Bordoni and Schneider [2008]. We find that regime transitions occur when the slab-ocean heat capacity is low [Geen et al., 2019] and axial-tilt is $\gtrsim 10°$ [Geen et al., 2020]. Using ITCZ metrics from Adam et al. [2016], we then attempt to characterize the decoupling of the precipitation maximum from the dividing streamline (i.e. the mid-tropospheric zero contour of the streamfunction).

## 1 Introduction

Monsoon systems are one of the most important large-scale systems in tropical and subtropical climate. Characterised by the seasonal reversal of winds, they are also harbingers of intense rainfall that are important to local and regional agrarian economies in many countries.

The global monsoon system has historically been likened to a planetary-scale land-sea breeze, with the land heating up more rapidly than the surrounding oceans due to its lower heat-capacity, thus forming regional lows that draw in moist air and result in higher precipitation [Halley, 1687]. However, many observations of global climate have been shown to diverge from this conventional view. For example, droughts tend to coincide with years with higher land-surface temperatures [Simpson, 1921], and land-sea temperature contrast is highest pre-monsoon onset, rather than during the monsoon itself [Kothawale and Kumar, 2002].

About a decade ago, Schneider and Bordoni [2008] showed that monsoons can occur in a spatially homogeneous Aquaplanet slab/swamp ocean (Fig. 1). Although the dynamics of monsoon systems on Earth are inevitably modified by regional topography and inhomogeneity, they are not truly necessary for monsoons to occur. Instead, it was proposed in Bordoni and Schneider [2008] that monsoons are eddy-mediated transitions between two atmospheric regime states: (1) an **equinoctal regime** where the Hadley circulation is controlled by eddy momentum fluxes, which in turn respond to thermal forcing, and (2) a **solstitial regime** where the Hadley circulation approaches the angular-momentum-conserving limit and therefore its strength directly responds to thermal forcing.

The interaction between the Hadley cell and mid-latitude eddies is summed up in an equation shown in Walker and Schneider [2006]:

$$(f+\overline{\zeta})\overline{v} = f(1-\mathrm{Ro})\overline{v} = \mathcal{S} \tag{1}$$

Where $\mathrm{Ro} = -\zeta/f$ is the local Rossby number, and $\zeta$ is the relative vorticity. The **equinoctal regime** corresponds to states where $\mathrm{Ro} \to 0$ (typically $\mathrm{Ro} \leq 0.2$), and the **solstitial regime** corresponds to when $\mathrm{Ro} \to 1$ (typically $\mathrm{Ro} \geq 0.5$) for the cross-equatorial winter cell. The rapid transition between both states is attributed to the limited ability of eddies to propagate into low latitudes, especially as the maximum meridional streamfunction of the cross-equatorial winter Hadley cell migrates across the equator into the summer hemisphere.

The behaviour of the ITCZ relative to the dividing streamline that denotes the boundary between the winter and summer Hadley Cells is also different in both regimes. In the **equinoctal regime**, the ITCZ is co-located with the dividing streamline. However, in the **solstitial regime**, the ITCZ gradually decouples from the dividing streamline and is found slightly

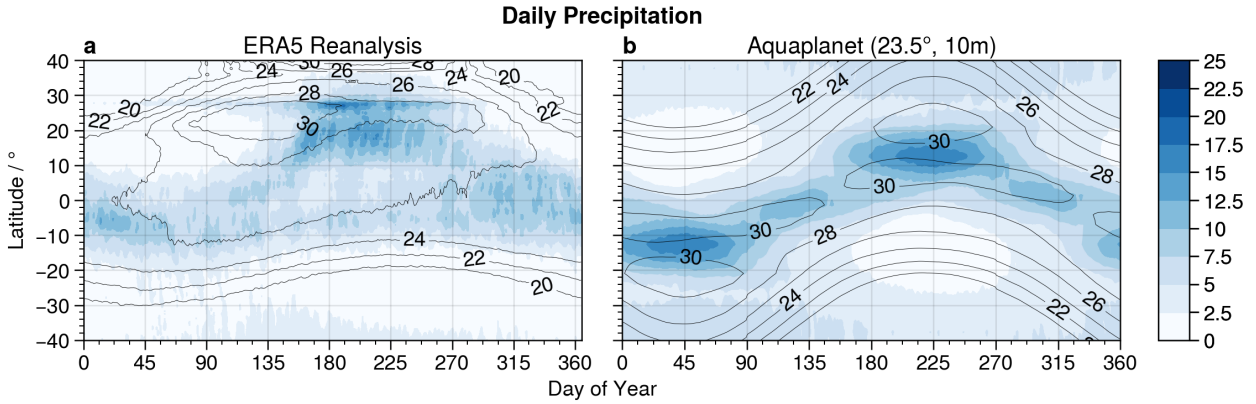


**Figure 1:** Contour plots of (blue,shaded) daily precipitation and (black,lines) surface temperature, with data taken from (a) ERA5 reanalysis and (b) an Aquaplaent simulation with axial tilt at 23.5° and slab-depth 10 m, in a manner similar to Fig. 1 of Bordoni and Schneider [2008].

equatorward, as illustrated in Fig. 2 (see also Geen et al. [2020]). In a method similar to Geen et al. [2019], I aim to investigate parameters in Aquaplanet GCMs, specifically axial tilt and slab-depth, that can affect the transition of idealised Hadley cells from the equinoctal regime to the solstitial regime.

Section 2 describes the GCM that was used in this project, as well as the methodology used to calculate and characterise the monsoonal behaviour. Section 3 details and discusses the results, while I summarise my conclusions in Section 4.

## 2 Methodology

### 2.1 GCM Experimental Setup

I used the "Isca" model framework to investigate the seasonal migration of the ITCZ and the Hadley cell. The model framework is described in Vallis et al. [2018] and allows me to easily and flexibly construct model hierarchies and experiments. The Isca Aquaplanet GCM is based off Frierson et al. [2006] with modifications to the gray atmosphere made by OGorman and Schneider [2008]. The model was run at the T42 resolution and 25 uneven $\sigma$-levels with a timestep of 720s. Similar to Frierson [2007], Bordoni and Schneider [2008] and Schneider and Bordoni [2008] we used the Shallow Betts-Miller scheme to parameterize moist convection in the tropics.

As with Bordoni and Schneider [2008], the surface of the Aquaplanet is a slab-ocean in order to close the atmospheric energy budget, which is different from the methodology of Schneider and Bordoni [2008], where they instead used Newtonian relaxation methods towards a fixed atmospheric profile. I do not parameterise ocean heat transport in this experiment, and it has been noted that this might result in Hadley cells that are stronger than Earths annual-mean for similar temperature profiles [OGorman and Schneider, 2008, Jucker and Gerber, 2017].

| Scheme | Configurations | Description |
|---|---|---|
| Control | | Default aquaplanet configuration without any land surface. |
| Axial Tilt / ° | 5, 10, 15, 20, 25 | Changes axial tilt / planetary obliquity |
| Slab Depth / m | 1, 2, 5, 10, 20 | Changes mixed-layer ocean heat capacity |

**Table 1:** The summary of the experimental configurations for this project.

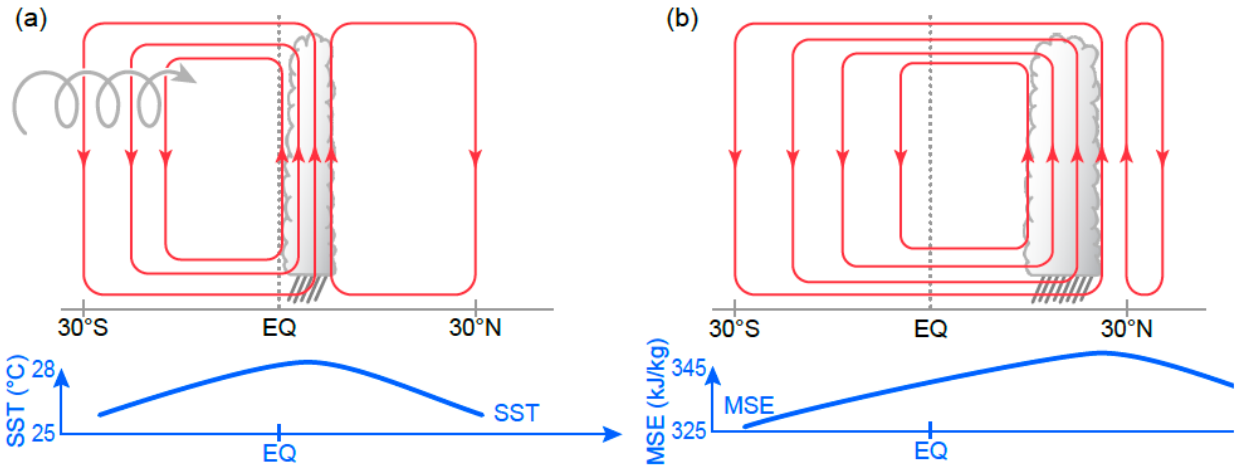


**Figure 2:** The regime states of the Hadley circulation: the (a) **equinoctal** regime, where eddy-momentum fluxes from the mid-latitudes limits the strength of the Hadley circulation, and the (b) solstitial regime, where the Hadley cell is approximately angular-momentum conserving. This figure was taken from Geen et al. [2020].

In this project, I varied the thickness of the slab-depth in order to change the responsiveness of the ocean to seasonal insolation. However, based on preliminary results (Fig. 5) it appears that Aquaplanets of slab depths $< \mathcal{O}(10\,\mathrm{m})$ shown pronounced transitions between the equinox and solstice regimes if the axial-tilt is pronounced enough. A list of the experiments conducted is shown in Table 1. The model was initially spun-up for 3-years of model-time without a seasonal insolation cycle, and then each experiment was run for 20 model-years based for each combination of axial-tilt and slab-depth listed. The solar constant was taken to be 1360 W $\mathrm{m}^{-2}$, and there is no diurnal cycle.

## 2.2 Centroid and Maximum Latitudes

The ITCZ and its migration has often been studied using the precipitation centroid latitude $\phi_{\text{P.cent}}$, first defined by Frierson and Hwang [2012] as:

$$\phi_{P.\text{cent}} = \frac{\int_{-20}^{20} \phi P(\phi) \cos\phi \, \mathrm{d}\phi}{\int_{-20}^{20} P(\phi) \cos\phi \, \mathrm{d}\phi} \tag{2}$$

The precipitation centroid $\phi_{\text{P.cent}}$ has been previously used to approximate the latitude of the precipitaton median $\phi_{\text{P.med}}$ which is defined to be where

$$\int_{-20}^{\phi_{P.\text{med}}} P(\phi) \cos\phi \, \mathrm{d}\phi = \int_{\phi_{P.\text{med}}}^{20} P(\phi) \cos\phi \, \mathrm{d}\phi$$

Although first defined to account only for precipitation within the tropics (20°S to 20°N) [Frierson and Hwang, 2012, Donohoe et al., 2013, Adam et al., 2016], Geen et al. [2019] extended the bounds of the integration range to 45° from the equator, and found that in a range of experiments similar to that covered by this project, changing the range of latitudes does not introduce significant bias from mid-latitude precipitation, and precipitation is still almost wholly dominated by the tropics (see Fig. 5 for verification).

In addition, Adam et al. [2016] also defined the precipitation maximum latitude $\phi_{\text{P.maxA}}$, given by

$$\phi_{P.\text{maxA}} = \frac{\int_{-20}^{20} \phi [P(\phi) \cos\phi]^N \, \mathrm{d}\phi}{\int_{-20}^{20} [P(\phi) \cos\phi]^N \, \mathrm{d}\phi} \tag{3}$$

The area-weighted precipitation was raised to power $N$ in $\phi_{\text{P.maxA}}$ such that $\phi_{\text{P.maxA}}$ would fall close to the precipitation maximum. Adam et al. [2016] found that $N = 10$ strikes a balance between emphasis on the maximum precipitation, while applying some smoothing to the discontinuities that arise

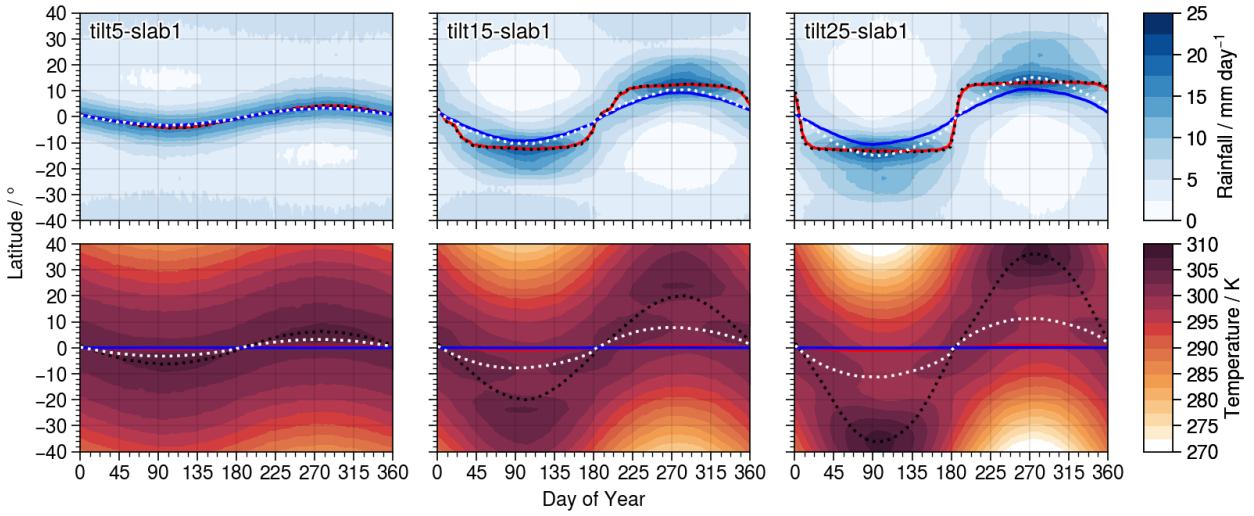


**Figure 3:** Contour plots of (top) daily precipitation and (bottom) surface temperature, for various aquaplanet configurations. Here, we also plot (black,dotted) $\phi_{\text{max}}$ as defined in Equations (4,6), (white,dotted) $\phi_{\text{cent}}$ as defined in Equations (4,6) but with $N = 1$ (i.e. centroid), (red,solid) $\phi_{\text{A.max}}$ as defined in Eqn. 3 [Adam et al., 2016] and (blue,solid) $\phi_{\text{cent}}$ as defined in Eqn. 2 [Frierson and Hwang, 2012]

when the precipitation maximum is directly identified. However, this overemphasizes the importance of area-weighting, as the $\cos\phi$ term is also raised to power $N$. Specifically, this method fails when the variability of $P$ is small compared to their average absolute values.

This is not usually a problem for precipitation, as the ITCZ has a prominent amplitude relative to the global average. But when we wish to extend this methodology to other variables, such as surface temperature, we find that Eqn. 3 fails. This is because variations in surface temperature are much smaller than the absolute value of area-weighted global-mean temperature. Thus Eqn. 3 would be dominated by variations in the weighted-area $\cos\phi$ instead of surface temperature.

Therefore, for the purposes of this project, I propose a modified version of this equation:

$$\phi_{X.\text{max}} = \frac{\int_{\phi_\text{S}}^{\phi_\text{N}} \phi X'(\phi)^N \cos\phi \,\mathrm{d}\phi}{\int_{\phi_\text{S}}^{\phi_\text{N}} X'(\phi)^N \cos\phi \,\mathrm{d}\phi} \qquad (4)$$

$$X' = X - \min(X)$$

This is a general formula that finds the area-weighted centroid and maximum values of variable $X$, integrated from the southern boundary $\phi_\text{S}$ to the northern boundary $\phi_\text{N}$. For Precipitation $P$ and Surface Temperature $T_s$, we take the following values of $N$, $\phi_\text{N}$ and $\phi_\text{S}$:

$$\phi_{P.\text{max}} = \{N = 10,\ \phi_\text{N} = 45°\text{N},\ \phi_\text{S} = 45°\text{S} \qquad (5)$$

$$\phi_{T_s.\text{max}} = \{N = 20,\ \phi_\text{N} = 90°\text{N},\ \phi_\text{S} = 90°\text{S} \qquad (6)$$

And we plot the curves in Fig. 3 for some sample experiments with pronounced tilt. We see that although our $\phi_{P.\text{max}}$ and $\phi_{P.\text{cent}}$ curves are very similar to the results expected from Adam et al. [2016], we are unable to capture the seasonal migration of surface temperature $T_s$ using Eqns. 2 and 3, but we are able to do so using Eqn. 4 and the bounds given in Eqn. 6.

## 3 Results and Discussion

### 3.1 Control Climatology

The average surface temperature of the **control** experiment is 290.8 K, has a single ITCZ peak centered about the equator. Other key characteristics of

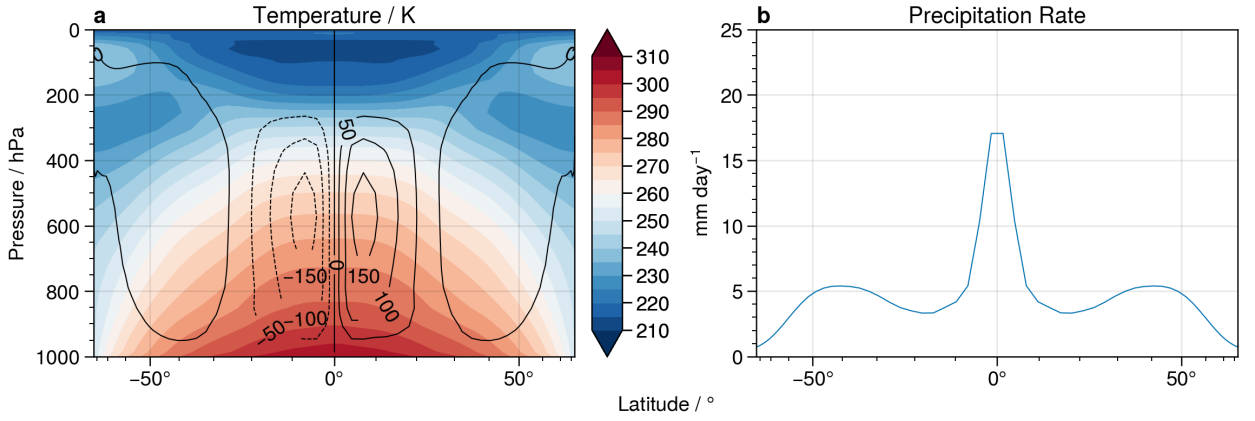


**Figure 4:** Mean climatology for the control aquaplanet simulation without axial tilt.

the control climatology (meridional streamfunction $\Psi$, precipitation and air temperature) are plotted in Fig. 4. The climatology of this aquaplanet is relatively similar to that found in previous baseline studies [OGorman and Schneider, 2008, Frierson, 2007] and therefore results from this project should be reproducible with margin of error.

### 3.2 Summary of Experimental Results

The results are summarised in Fig. 5, which shows the seasonal climatology for representative configurations among the experiments conducted, and Fig. 6, which plots the seasonal variability of $\Psi_{500}$, which is the meridional streamfunction at the $\sigma$-level corresponding to the mid-troposphere at 500 hPa. I also plot $\phi_{P.\max}$ and $\phi_{T_s.\max}$ and compare their seasonal migration with that of the $\Psi_{500} = 0$ curve. It can be qualitatively seen that aquaplanets with higher axial tilt and lower slab depth show sharp and discontinuous transitions between two climatological regimes, which are taken to be the **equinoctal** and **soltitial** regimes. However, aquaplanets with either axial tilt $< \mathcal{O}(10°)$ or slab depth $> \mathcal{O}(5\text{ m})$ generally show only smooth fluctuations within a roughly **equinoctal** regime.

It is qualitatively observable from Fig. 5 and distinctly clear in Fig. 6 that $\phi_{P.\max}$ decouples from the dividing streamline between the Hadley Cells, approximated by $\phi_{\Psi_{500}} = 0$. In fact, I see from Fig. 6 that regardless of axial tilt, $\phi_{P.\max}$ plateaus at $\sim$ 13°N/S. Previous studies have found that the ITCZ migrates farther polewards than this latitude, but this is likely partially because previous studies used $\phi_{P.\text{cent}}$, the centroid latitude, which captures the presence of a bifurcation in the ITCZ that occurs during the solstitial regime.

In contrast I see that $\phi_{T_s.\max}$ is able to better capture the migration of the curve $\phi_{\Psi_{500}} = 0$ during the solstitial regime (Fig. 6). During the solstitial regime, the migration of $\phi_{\Psi_{500}} = 0$ tends to follow the maximum curve for Moist Static Energy (MSE) [Geen et al., 2020], but due to time constraints I assume that $\phi_{T_s.\max}$ is able to approximate the $\phi_{\Psi_{500}} = 0$ curve.

An example cross-section of the equinoctal- and solstitial-regime atmospheric circulations are shown in Fig. 7. Similar to Fig. 2, It can be seen that in the equinoctal regime, both $\phi_{T_s.\max}$ and $\phi_{P.\max}$ roughly coincide with the terminus of the Hadley circulation. However, during the solstitial regime, $\phi_{T_s.\max}$ and $\phi_{\Psi_{500}} = 0$ are both strongly decoupled from $\phi_{P.\max}$. It can also be seen that $\phi_{T_s.\max}$ is also located close to the terminus of the Hadley circulation in the solstitial-regime, similar to the MSE in Fig. 2 [Geen et al., 2020]. During the solstitial regime, the strength of the cross-equatorial Hadley circulation is much stronger than that typically found on Earth, perhaps due to the lower surface friction in an aquaplanet world? Or possibly this could also be a

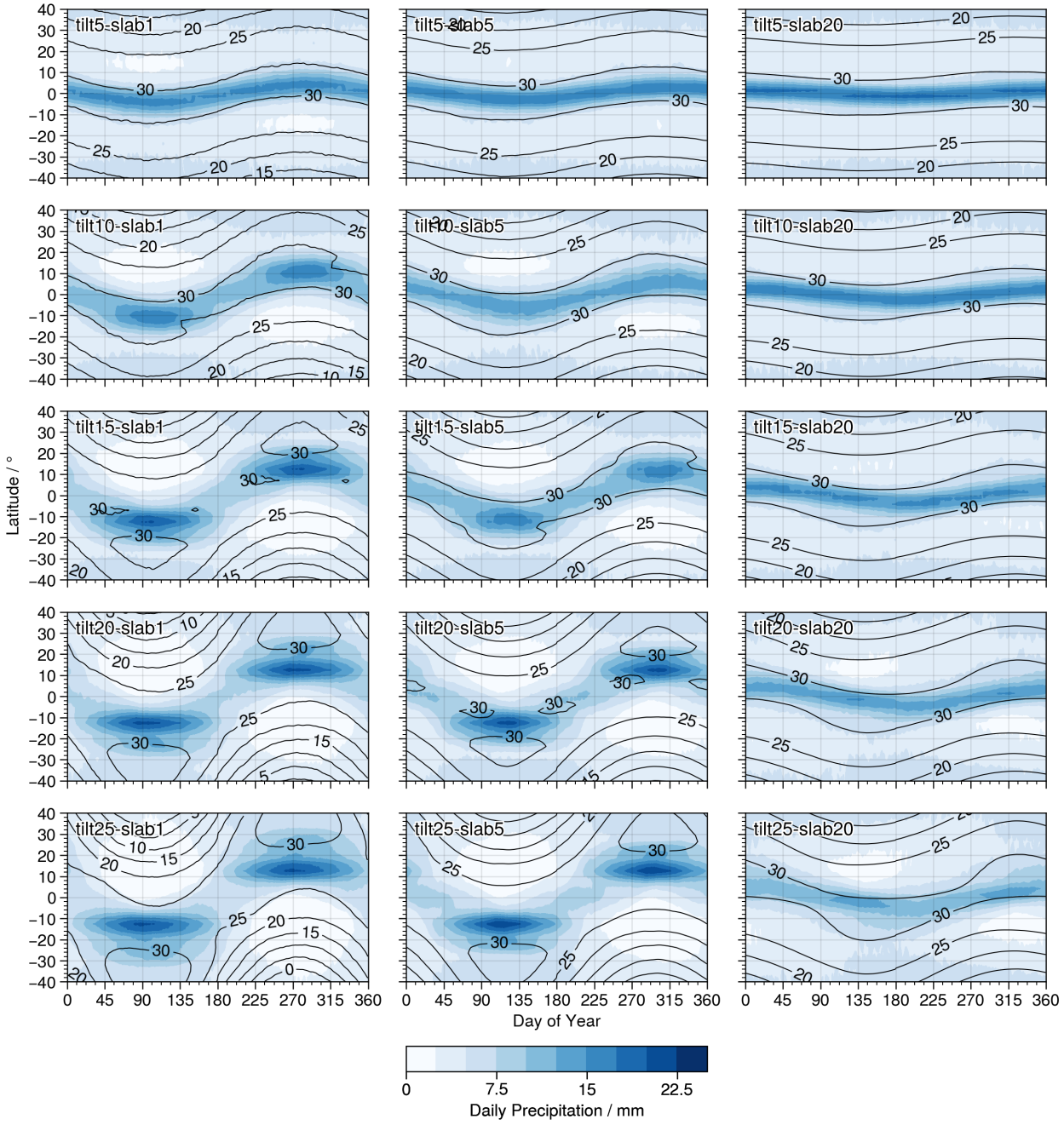


**Figure 5:** The seasonal variability of (blue,shaded) daily precipitation and (black,lines) surface temperature for different aquaplanet configurations.

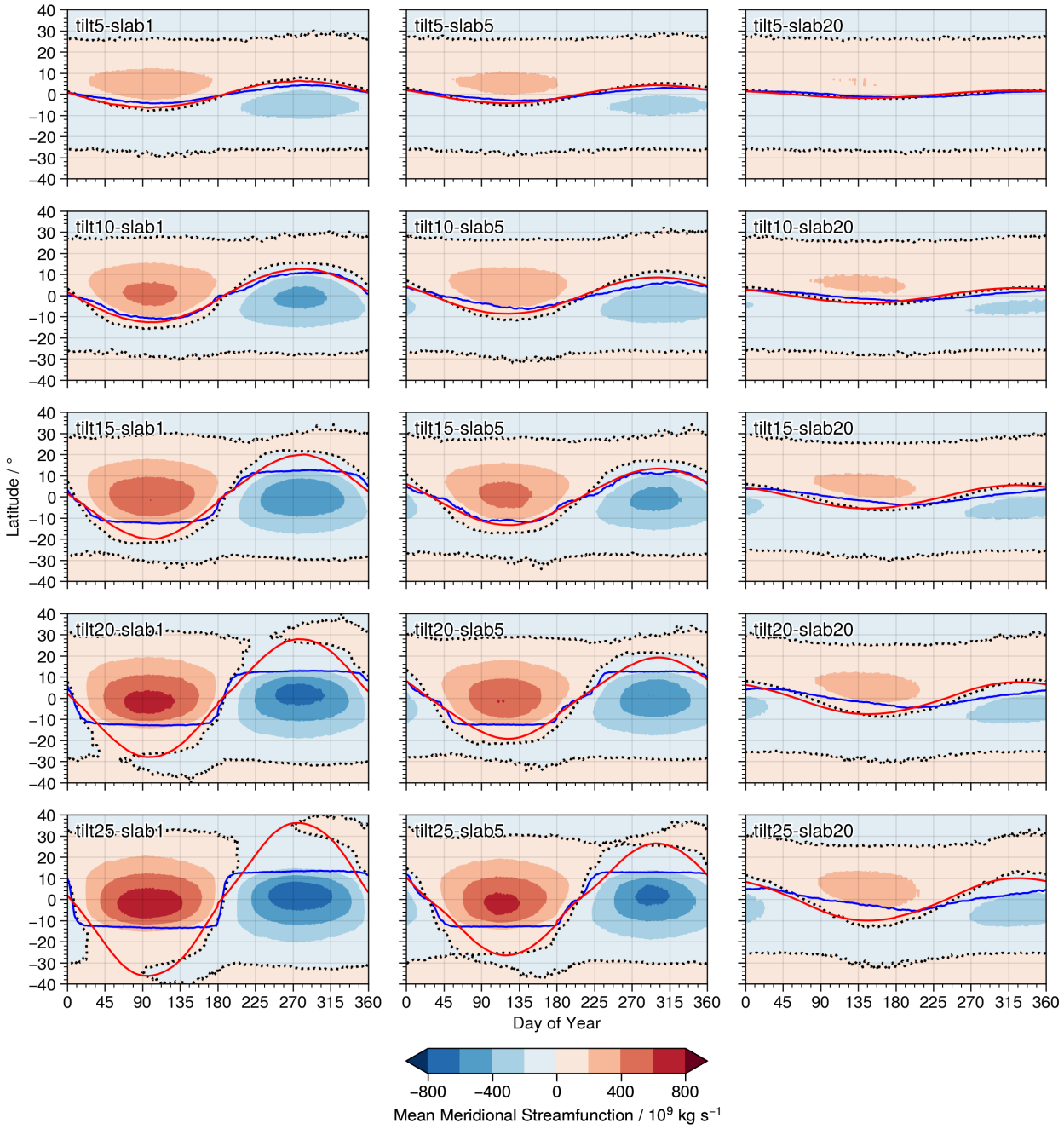


**Figure 6:** The seasonal variability of (shaded) zonal-mean meridional streamfunction at the $\sigma$-level closest to 500 hPa ($\Psi_{500}$), (black,dotted) the dividing streamline for $\Psi_{500} = 0$, (blue,solid) $\phi_{P.\max}$ and (red,solid) $\phi_{T_s.\max}$.

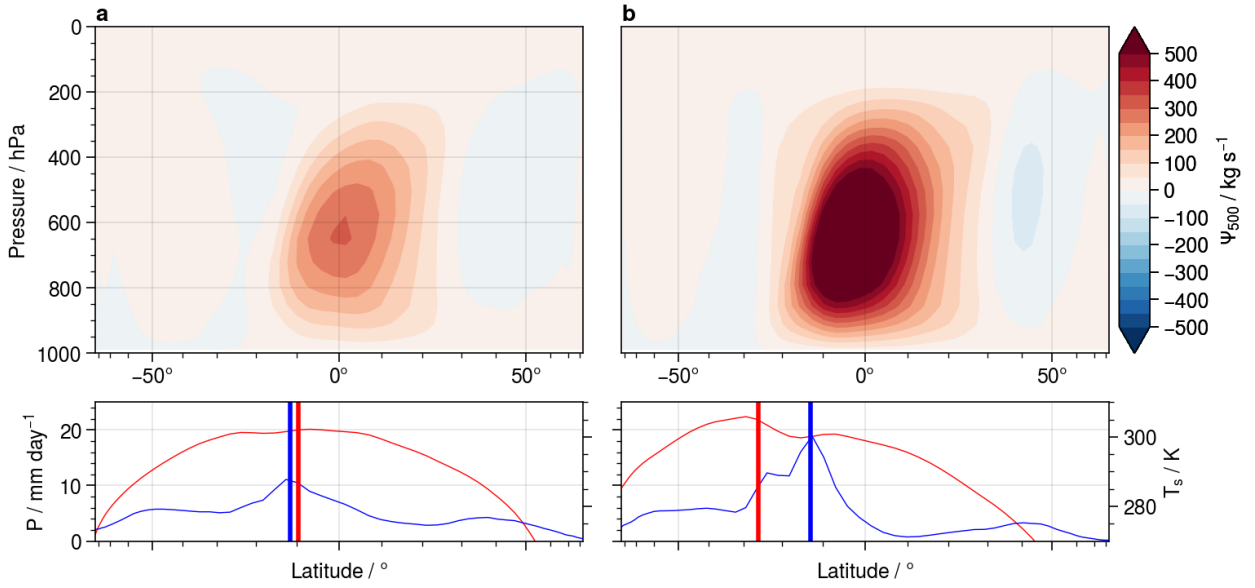


**Figure 7:** Snapshot of the zonal-mean climatology for the (a) equinoctal and (b) solstitial regimes. For the line plots below, we plot (red) surface temperature $T_s$ and precipitation $P$. Thick vertical lines represent $\phi_{X.\max}$ for each respective variable.

feature due to using grey radiation, as different radiative schemes have been known to have impacts on the tropospheric climate such as the jet stream.

### 3.3 Solstitial-Equinoctal Transitions

From Fig. 6, it becomes apparent that not all configurations transition between both and equinoctal state and a solstitial state. Configurations with high slab-ocean heat capacity have an atmospheric circulation in a permanent equinoctal state. Aquaplanets with low slab-ocean heat capacity, however, may be found in a permanent equinoctal state, transition between both the solstitial and equinoctal state depending on heat distribution, or settle into a permanent solstitial state depending on the magnitude of their axial tilt.

The nature of this transition can be investigated by plotting $\partial_t \phi_{X.\max}$ (the rate of displacement of $\phi_{X.\max}$) against $\phi_{X.\max}$ itself (see Fig. 8) in a manner similar to that performed by Geen et al. [2019]. We see from the plots of $\phi_{P.\max}$ against $\partial_t \phi_{P.\max}$ that when slab-depth and/or axial-tilt are moderate, the atmospheric regime oscillates not only between two different solstitital states, but also with an equinoctal state. Furthermore, we see that the transition between the solstitial and equinoctal states (where both states are shown to occur) is very rapid. We also note that within these states, $\partial_t \phi_{P.\max} \approx 0$, which means that the atmospheric equinoctal state tends to be stable rather than oscillatory.

Therefore, from Fig. 8, we establish the following criteria to determine if an aquaplanet is in a solstitial or equinoctal state based on $\phi_{P.\max}$:

(1) If $|\phi_{P.\max}| > 10°$, $|\partial_t \phi_{P.\max}| < 0.25°$ day$^{-1}$, then the atmospheric state is **solstitial**.

(2) If the atmospheric state is never **solstitial**, then the atmosphere is in a **perpetual equinoctal** state.

(3) If $|\phi_{P.\max}| \leq 5°$, $|\partial_t \phi_{P.\max}| < 0.25°$ day$^{-1}$, then the atmosphere is in an **equinoctal** state.

(4) In all other cases, the atmosphere is in a state of **transition**.

I then plot the frequency at which these states occur in the atmosphere in Fig. 9. We see that though

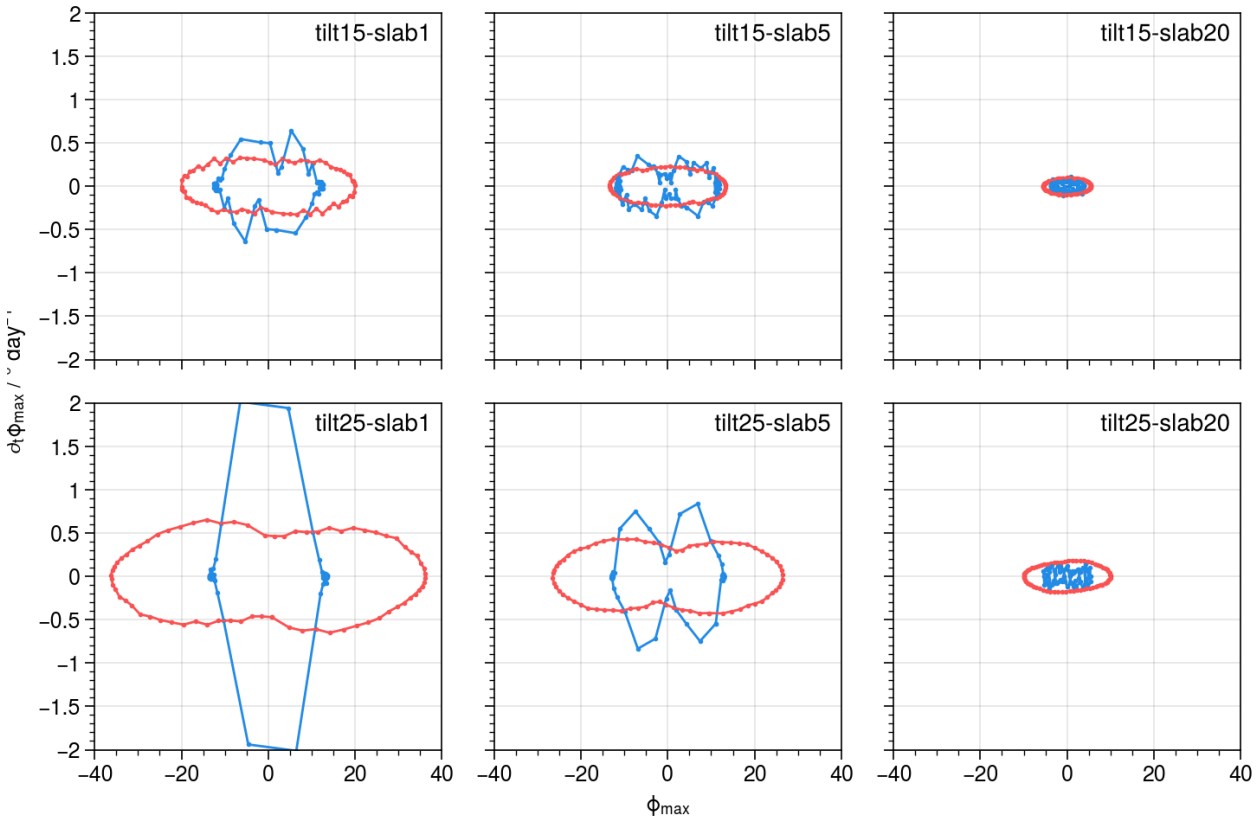


**Figure 8:** Plots of $\phi_{\max}$ against $\partial_t \phi_{\max}$

the atmospheric circulation is mostly found in either the solstitial or equinoctal regimes, there are certain combinations, especially at axial tilt $\sim 10°$ where the atmospheric state is found in transition between those states, perhaps because the atmosphere on the boundary between transitioning towards a solstitial state, if only for a short period of time.

## 4 Conclusion and Future Work

Much of the work done in this project is very preliminary. A more thorough analysis needs to be done, with more experiments covering axial-tilt and slab-depth in greater resolution in order to properly analyze the regime transitions for intermediate states.

We also find that the strength of the Hadley cell in the solstitial states in our aquaplanet experiments is much greater than on Earth. I am currently uncertain as to the cause, but I hope to explore different radiation settings that can be found within Isca.

## Addendum

Most of the codes specific to this project are available on in the GitHub repository: https://github.com/natgeo-wong/MonsoonTilt. This includes experimental configurations for the Isca GCM. The source code for the Isca GCM can be found at https://github.com/ExeClim/Isca, and `IscaTools.jl`, which is used for basic preliminary analysis and calculation of zonal-mean meridional stremfunctions, can be found at https://github.com/natgeo-wong/IscaTools.jl.

## References

O. Adam, T. Bischoff, and T. Schneider. Seasonal and Interannual Variations of the Energy

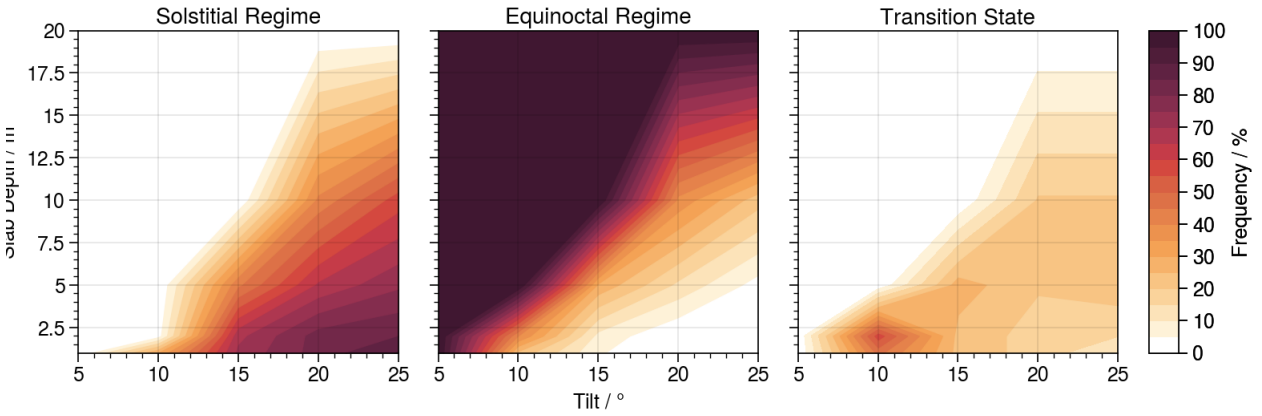


**Figure 9:** Frequency of the different regimes in different aquaplanet configurations.

Flux Equator and ITCZ. Part II: Zonally Varying Shifts of the ITCZ. *Journal of Climate*, 29 (20):7281–7293, 10 2016. ISSN 0894-8755. doi: 10.1175/JCLI-D-15-0710.1. URL http://journals.ametsoc.org/doi/10.1175/JCLI-D-15-0710.1.

S. Bordoni and T. Schneider. Monsoons as eddy-mediated regime transitions of the tropical overturning circulation. *Nature Geoscience*, 1(8):515–519, 8 2008. ISSN 1752-0894. doi: 10.1038/ngeo248. URL http://www.nature.com/articles/ngeo248.

A. Donohoe, J. Marshall, D. Ferreira, and D. Mcgee. The Relationship between ITCZ Location and Cross-Equatorial Atmospheric Heat Transport: From the Seasonal Cycle to the Last Glacial Maximum. *Journal of Climate*, 26(11):3597–3618, 6 2013. ISSN 0894-8755. doi: 10.1175/JCLI-D-12-00467.1. URL http://journals.ametsoc.org/doi/10.1175/JCLI-D-12-00467.1.

D. M. W. Frierson. The Dynamics of Idealized Convection Schemes and Their Effect on the Zonally Averaged Tropical Circulation. *Journal of the Atmospheric Sciences*, 64(6):1959–1976, 6 2007. ISSN 0022-4928. doi: 10.1175/JAS3935.1. URL http://journals.ametsoc.org/doi/abs/10.1175/JAS3935.1.

D. M. W. Frierson and Y.-T. Hwang. Extratropical Influence on ITCZ Shifts in Slab Ocean Simulations of Global Warming. *Journal of Climate*, 25 (2):720–733, 1 2012. ISSN 0894-8755. doi: 10.1175/JCLI-D-11-00116.1. URL http://journals.ametsoc.org/doi/10.1175/JCLI-D-11-00116.1.

D. M. W. Frierson, I. M. Held, and P. Zurita-Gotor. A Gray-Radiation Aquaplanet Moist GCM. Part I: Static Stability and Eddy Scale. *Journal of the Atmospheric Sciences*, 63(10):2548–2566, 10 2006. ISSN 0022-4928. doi: 10.1175/JAS3753.1. URL http://journals.ametsoc.org/doi/abs/10.1175/JAS3753.1.

R. Geen, F. H. Lambert, and G. K. Vallis. Processes and Timescales in Onset and Withdrawal of Aquaplanet Monsoons. *Journal of the Atmospheric Sciences*, 76(8):2357–2373, 8 2019. ISSN 0022-4928. doi: 10.1175/JAS-D-18-0214.1. URL http://journals.ametsoc.org/doi/10.1175/JAS-D-18-0214.1.

R. Geen, S. Bordoni, D. S. Battisti, and K. L. Hui. The dynamics of the global monsoon: Connecting theory and observations. *Earth and Space Science Open Archive*, page 50, 2020. doi: 10.1002/essoar.10502409.1. URL https://doi.org/10.1002/essoar.10502409.1.

E. Halley. An historical account of the trade winds, and monsoons, observable in the seas between and near the Tropicks, with an attempt to assign the physical cause of the

said winds. *Philosophical Transactions of the Royal Society of London*, 16(183):153–168, 12 1687. ISSN 0261-0523. doi: 10.1098/rstl.1686.0026. URL https://royalsocietypublishing.org/doi/10.1098/rstl.1686.0026.

M. Jucker and E. P. Gerber. Untangling the Annual Cycle of the Tropical Tropopause Layer with an Idealized Moist Model. *Journal of Climate*, 30 (18):7339–7358, 9 2017. ISSN 0894-8755. doi: 10.1175/JCLI-D-17-0127.1. URL http://journals.ametsoc.org/doi/10.1175/JCLI-D-17-0127.1.

D. Kothawale and K. R. Kumar. Tropospheric temperature variation over india and links with the indian summer monsoon: 1971-2000. *Mausam*, 53 (3):289–308, 2002.

P. A. OGorman and T. Schneider. The Hydrological Cycle over a Wide Range of Climates Simulated with an Idealized GCM. *Journal of Climate*, 21 (15):3815–3832, 8 2008. ISSN 0894-8755. doi: 10.1175/2007JCLI2065.1. URL http://journals.ametsoc.org/doi/abs/10.1175/2007JCLI2065.1.

T. Schneider and S. Bordoni. Eddy-Mediated Regime Transitions in the Seasonal Cycle of a Hadley Circulation and Implications for Monsoon Dynamics. *Journal of the Atmospheric Sciences*, 65(3):915–934, 3 2008. ISSN 0022-4928. doi: 10.1175/2007JAS2415.1. URL http://journals.ametsoc.org/doi/abs/10.1175/2007JAS2415.1.

G. C. Simpson. The Origin of the South-west Monsoon. *Nature*, 107(2683):154–154, 3 1921. ISSN 0028-0836. doi: 10.1038/107154a0. URL http://www.nature.com/articles/107154a0.

G. K. Vallis, G. Colyer, R. Geen, E. Gerber, M. Jucker, P. Maher, A. Paterson, M. Pietschnig, J. Penn, and S. I. Thomson. Isca, v1.0: a framework for the global modelling of the atmospheres of Earth and other planets at varying levels of complexity. *Geoscientific Model Development*, 11(3):843–859, 3 2018. ISSN 1991-9603. doi: 10.5194/gmd-11-843-2018. URL https://www.geosci-model-dev.net/11/843/2018/.

C. C. Walker and T. Schneider. Eddy Influences on Hadley Circulations: Simulations with an Idealized GCM. *Journal of the Atmospheric Sciences*, 63(12):3333–3350, 12 2006. ISSN 0022-4928. doi: 10.1175/JAS3821.1. URL http://journals.ametsoc.org/doi/10.1175/JAS3821.1.